The tunable resonant IC antenna concept and its design for DTT experiment

PAPER • OPEN ACCESS

The tunable resonant IC antenna concept and its design for DTT experiment

To cite this article: D. Milanesio *et al* 2024 *Nucl. Fusion* **64** 016015

OPEN ACCESS
IOP Publishing | International Atomic Energy Agency
Nuclear Fusion
Nucl. Fusion **64** (2024) 016015 (10pp)
https://doi.org/10.1088/1741-4326/ad0c7f

The tunable resonant IC antenna concept and its design for DTT experiment

D. Milanesio[1,*], D.L. Galindo Huertas[1], S. Ceccuzzi[2,3], G. Vecchi[1], B. Baiocchi[4], A. Cardinali[2], D. Mascali[5], G.S. Mauro[5], F. Mirizzi[6], A. Pidatella[5], G.L. Ravera[2], G. Torrisi[5] and A.A. Tuccillo[6]

[1] Politecnico di Torino, Dipartimento di Elettronica, Torino, Italy
[2] ENEA, Frascati, Italy
[3] DTT S.C. a r.l., Frascati, Italy
[4] CNR-ISTP, Milano, Italy
[5] INFN-LNS, Catania, Italy
[6] Consorzio CREATE, Napoli, Italy

E-mail: daniele.milanesio@polito.it

Received 8 May 2023, revised 25 October 2023
Accepted for publication 14 November 2023
Published 23 November 2023

Abstract

The intrinsic poor loading of Ion Cyclotron (IC) plasma-facing antennas makes the use of Tuning and Matching Systems (TMSs) a necessity. The antenna plus TMS is a resonant system; in the TMS and access lines high voltages (tens of kV) must be accounted for in the unavoidable unmatched part of the feeding lines. In this work, we propose and test an innovative type of IC launcher; it is based on achieving resonance of the self-standing antenna, i.e. without the TMS. A mechanical full-metal tuning mechanism is described and demonstrated to allow wide-band operation. A systematic analysis of possible antenna topologies has led to identifying a structure that can allow good impedance matching along with compliance with maximum electric field constraints. Most of the design is carried out using a simplified plasma and a commercial analysis tool and then validated with a realistic plasma using TOPICA code.

Keywords: DTT, ICRF antenna, ICRF heating, resonant antenna, TOPICA

(Some figures may appear in colour only in the online journal)

1. Motivation and background

Among the auxiliary systems adopted in present-day experiments towards the realisation of controlled nuclear fusion with magnetic confinement, Ion Cyclotron (IC) antennas are certainly one of the most promising options to deliver high power to the plasma. As a matter of fact, IC antennas are currently installed and routinely operated in almost all the existing fusion experiments and are foreseen for the next generation of tokamaks like ITER, SPARC [1] and DEMO [2]. An IC system is to be designed also for the Divertor Tokamak Test facility (DTT) [3–5], a new tokamak under realization at the ENEA Frascati Research Center.

Unfortunately, IC launchers, if compared to antennas used in radars or telecommunications, are definitely characterised by very poor loadings, i.e. by very high reflection coefficients at their input ports. To be more specific, the working frequency (usually of the order of tens of MHz), the high power to be delivered to plasma, the limited space available on the

* Author to whom any correspondence should be addressed.

machines and, in general, the mechanical constraints do not allow to easily reach an efficient antenna design. This practically means that, for IC systems to be successfully operated in plasma fusion experiments, extremely high voltage values have to be imposed along the input lines, between the antenna and the mandatory matching system. As one may guess, high voltages are rather dangerous for both the feeding lines, leading to breakdowns, especially at the feedthroughs, and for the antenna itself, above all around the radiating elements, causing arcs and driving RF potentials that can eventually damage the entire system.

Given these conditions, even a small reduction of the input reflection coefficient would determine a remarkable gain in terms of power transferred to plasma (at constant voltage) or, even better, a consistent decrease of the input voltage (at constant delivered power). The aim of this work is to introduce and describe an innovative antenna concept based on a self-resonant structure for the upcoming DTT experiment; to achieve the desired frequency band of operation, the antenna is made mechanically tunable. It is important to mention here that this paper would like to provide a proof of principle and not a complete antenna design; the mechanical, thermal and nuclear stresses should be addressed in a future paper.

The organisation of this paper is as follows: in section 2 an overview of the self-resonant tunable concept is provided, while section 3 contains the description of the adopted tools (section 3.1), of the simulated preliminary geometries (section 3.2) and a detailed analysis of the optimized launcher (sections 3.3–3.5).

2. Tunable resonant antennas

As well known [6], a (one port) structure is defined to be resonant if its input impedance $Z_{\rm in}(f)$ is purely real at the reference frequency f_0, i.e. $\mathrm{Im}Z_{\rm in}(f_0) = 0$, $Z_{\rm in}(f_0) = R$. This remarkable property alone is not yet enough to make it practically usable; one also needs that the value of the real impedance at the resonance frequency matches the desired value set by generators and feeding line, R_0; the latter in typical IC systems is of the order of tens of Ohms (it is going to be $R_0 = 30\,\Omega$ for DTT IC antenna).

In typical IC antennas, the resonance is generally achieved after the Tuning and Matching System (TMS) located outside the vacuum chamber, as the antenna alone cannot reach this condition. A self-resonant antenna, on the contrary, is characterized by this property at its own port, thus relaxing the task of the TMS or dispensing it altogether.

It is well known that the (self) resonance of antennas happens when the electrical length is comparable to the wavelength; in a first approximation, we can employ here the vacuum wavelength $\lambda \approx \lambda_0 = c/f$, with the (small) impact of plasma discussed later on. For conventional types of antenna the first resonance happens for a length L of the antenna $L \approx \lambda_0/2$; this requires sizes typically not available in most machines, including DTT. For example, if the strap topology corresponds to a loop-type antenna, the typical resonance happens when the loop perimeter is $L_{\rm loop} \approx \lambda$; the strap is actually a half-loop, with the surrounding 'ground plane' accounting for the other half by image theorem, thus implying $L_{\rm strap} \approx \lambda/2$.

A resonance at a shorter antenna length is present for some antenna topologies (e.g. [7]) at $L \approx \lambda/4$ or shorter values for antennas loaded with some materials, whose viability in a tokamak environment has however to be ascertained.

The quarter-wavelength (QW) resonance happens for two fundamental topologies that are schematically depicted in figure 1:

(a) the loop, i.e. with $L_{\rm loop} \approx \lambda/2$ and $L_{\rm strap} \approx L_{\rm loop}/2 \approx \lambda/4$;
(b) the 'L-type' antenna, with $L_L \approx \lambda/4$ (its name refers to its resemblance to the L letter).

The half-wavelength-perimeter resonance of the loop happens irrespective of the loop shape, e.g. for a circular, square, or strap-like. It can be observed that when the loop-type is over a ground plane, there is an apparent duality between the (half) loop and the L-type, more evident when considering them as 'stubs' of a TL: the loop is terminated on a short, the L is terminated on an open; in the $L/\lambda \ll 1$ limit the loop exhibits an inductive behaviour whereas the L a capacitive one. Likewise, neglecting material and radiation losses at the QW resonance one expects $Z_{\rm in} \to \infty$ for the loop (short to open) and $Z_{\rm in} \to 0$ for the L (open to short); considering (small) radiation losses, one then expects to have a (very) small impedance for the L, and a (very) large one for the loop. Hence, it is evident that these 'primal' topologies must be augmented by a structure that allows them to bring their resonance impedance to a practical value.

Also, a relevant question is on which bandwidth this input impedance remains as close as required to the desired value. It is a classical result of antenna theory that this impedance bandwidth is proportional to the antenna volume measured in λ^3 [6]. Hence, all resonant small antennas are narrow-band. The typical required operational bandwidth of the ICRH system is in the order of 2:1 (e.g. in DTT from 60 to 90 MHz); as a result, a resonant antenna needs to be also complemented by a *structural* tuning mechanism.

For reasons that cannot be expounded in full here, employing the QW of loop-type is more difficult than for the L-type in the context of ICRH (mostly for the impedance matching and tuning requirements). The L-topology is more favoured even in communication antennas, that have less complex requirements than in plasma heating; the usual impedance matching structure, depicted in figure 1(*C*), is called the inverted-F antenna; as for the L name, this derives from the resemblance to the 'F' letter. The impedance matching structure is often described in terms of TLs, but this is inaccurate (and sometimes misleading) when the matching length x is small and comparable to the height h, which is often the case, especially in the applications of present interest; in this case, the closed current path formed from the feed point to the first ground short has instead

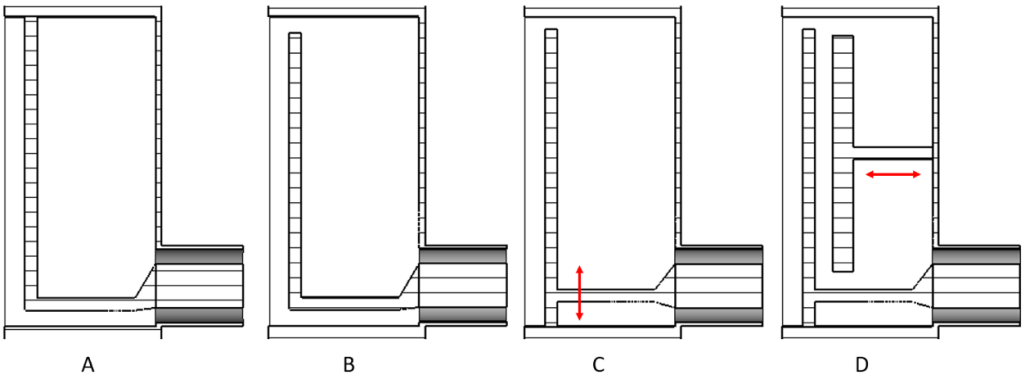

Figure 1. Poloidal cut of the resonant antenna. (*A*) Loop type ('strap'); (*B*) basic *L*-type; (*C*) inverted-F topology with impedance matching; (*D*) proposed structure with a tuning element. (Faraday shield omitted).

to be considered via magnetic inductive coupling, essentially amounting to an autotransformer. This will not be pursued analytically here; instead, it will be conveniently designed by means of parametric simulations as described in section 3.

The frequency tuning mechanism has to be compatible with the ICRH antenna environment; for example, variable capacitors have been excluded (they would be a very flexible tuning and matching, as was in the TORE-SUPRA case, which employed a loop-type resonance). Once at full performance, DTT will undergo activation and the remote handling system shall be used for all maintenance operations in the tokamak hall. JET experience taught that variable capacitors may need maintenance and/or fixings during their lifetime. Moreover, DTT frequency range is higher than some other machines, so we cannot use exactly the same capacitors of JET, WEST, or W7-X, but something different with fewer experimental records of its use in a tokamak. Such reasons made the capacitors appear partially risky in terms of reliability and maintainability and led to exclude their use. The envisioned system is schematically depicted in figure 1(*D*). It is based on the principle of changing the per-unit-length capacitance of the transmission line (TL); this does not impact the phase velocity (in the absence of dielectrics it is always the light velocity, c), but it impacts the characteristic impedance, and hence (for a given radiation loading) the (complex) input impedance; as the impedance matching structure is not changed, in this way the inductive-to-capacitive resonance balance happens at different frequencies. Its full description beyond the simple principle stated above calls for multi-conductor TL theory, and will not be pursued analytically here; the same holds for the impact of the Faraday shield.

An important remark should be pointed out with respect to the structures schematically shown in figure 1; at a first glance, structures (*B*)–(*D*) (especially the latter) resemble capacitors, fixed or variable. It has to be stressed that these structures *are not* such; in the first place these are *resonant* structures, which at the lowest order implies balancing of capacitance and inductance; second, the electrical lengths are between 1/8 and 1/4 wavelengths, and distributed capacitance and inductance are key to the actual functioning of these antennas.

Finally, we observe that the search for a self-resonant antenna for ICRH led to the solution described in [8] (and related papers). While that approach shares the same motivation of this work, the two concepts, and the resulting antennas, are very different. The approach in [8] was based on a loop antenna configuration, made to resonate by a suitable assembly of metal and dielectric elements; in that design, the presence of a dielectric layer (totally absent in this proposed concept) turned out quite challenging in terms of weight and manufacturing.

An important issue in ICRH antennas is power handling in terms of the maximum electric field. As well-known, electric field distribution is tied to the (time-averaged) stored electric energy, which is its volume integral. In turn, the resonance condition corresponds to the stored electric and magnetic energies being equal in magnitude thereby cancelling out due to their opposite sign. For a given energy, the minimum of the maximum field corresponds to having a constant field. This cannot be achieved in practice, and the sources of high field must be understood and their occurrence limited. It is well known that the E field on isolated conductors has a singular behaviour that is related to the geometrical asperity; in particular, for non-zero curvature radii, the field is inversely proportional to the local radius of curvature. This behaviour is modulated by the potential at each given point; hence, based on TL theory one expects the open end to be a critical part (the TL voltage is maximum at opens); a way of reducing the field hot spots is then rounding the edges and making the conductor thick.

3. Analysis of topologies for the tunable resonant IC launcher

We will now analyse the tunable self-resonant launcher described in section 2. We set as our main goals the possibility of tuning the antenna throughout the entire frequency range of DTT use, i.e. from 60 MHz to 90 MHz [9], and to be able to operate it at full power (1.5 MW per antenna, i.e. two straps) with maximum electric fields within the antenna box

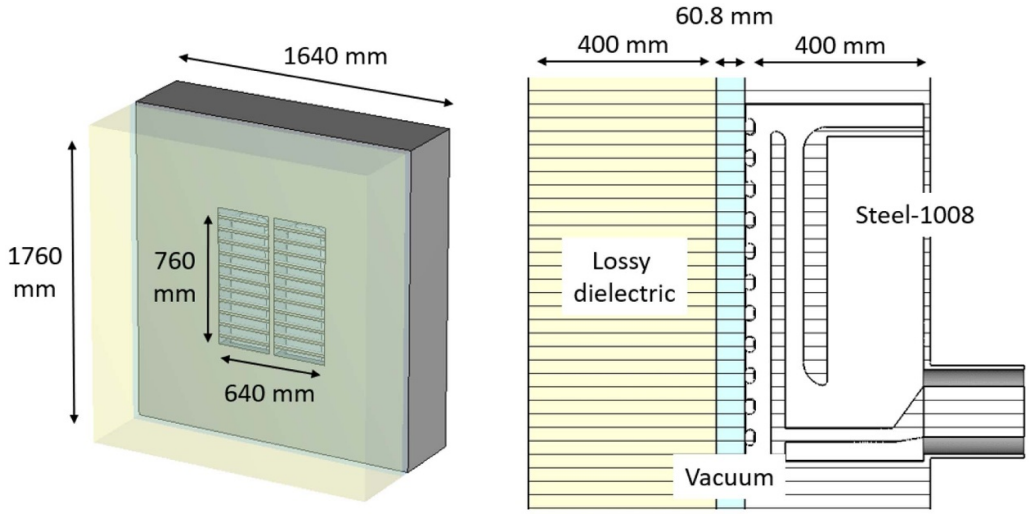

Figure 2. Front view (left) and poloidal cut (right) of the setup adopted in CST-MWS with some relevant dimensions (in millimetres). The two-straps antenna is enclosed within a box (all metallic elements are assumed to be Steel-1008) and located in front of a 60.8 mm vacuum layer followed by a 400 mm lossy dielectric.

around 2.5 MV m^{-1}. This field requirement in DTT derives from the experimental evidence and design requests of other machines (see table 1 in [4]). The broad frequency range is needed to locate the cyclotron resonances of 3 He (60 MHz) and H (90 MHz) minorities on the tokamak axis with the nominal DTT magnetic field of 5.85 T [4]. In terms of antenna feeding, we rounded up the input power per strap to 800 kW (instead of 750 kW) to have margin against antenna and TL losses. With respect to the foreseen generators layout depicted in [4], one could modify it and directly connect each generator to a strap if stable operating points were achievable and the antenna confirmed its ELM-resilient behaviour; an external system based on 3 dB hybrid couplers represents our last resort choice in case the use of additional hardware is unavoidable. Other details concerning the full IC system design can be found in [4].

3.1. Adopted tools and simulations setup

Figure 2 describes the setup adopted in CST-MWS to first select the most promising geometrical solution and then to properly optimize its performance. The 'equivalent' loading (right-hand side of the picture) was originally selected by minimizing the differences between CST-MWS and TOPICA simulations performed with the antenna geometry and the plasma profile adopted for the TOPICA preliminary DTT IC antenna design [10]. To be more specific, a 60.8 mm vacuum layer is located right in front of the Faraday Screen (FS) outer surface; a user-defined lossy dielectric ($\epsilon_r = 225$ and $\tan\delta = 1.17$ at 90 MHz) extends for additional 400 mm. The authors are hence aware that a different application both in terms of geometry and plasma loading may lead to slightly different outcomes.

A single strap/cavity was adopted throughout the entire optimization process (assuming 800 kW of input power), while the full launcher (two straps) was eventually simulated in TOPICA (see section 3.5). At this stage, no geometrical optimization was carried out on the FS. Several simulations with and without it, changing the number of bars and their section, were performed in [11], showing rather stable results in terms of resonance position and a small variation on electric fields maxima. Similarly, the RF contacts needed for the tuning element (TE) have not been optimized yet. The short pulse duration (about 50 s) and the first estimates of the current on the surface of the pole (about 1.5 kA) allows us to be quite optimistic about their usage.

3.2. Concept selection and antenna optimization

By observing figure 2, the reader can notice that, since the total dimensions are constant (they are bounded by the size of the port plug), only two elements are left for optimization, namely the strap and the TE. While addressing the interested reader to [11] for a detailed analysis of the simulated raw (not optimized) geometries, we shortly summarize here the selection process' rationale.

Figure 3 reports a poloidal cut of the most relevant tested geometries in terms of strap shape, keeping constant a standard TE with an asymmetric pole (labelled as TE2 in figure 4). The strap was modelled as an 'L-type' antenna (S1), shorted on one end in the front of the antenna box (S2a, S3) or in the back (S2b), shorted on more than one point in the front (S4a) or at the antenna back wall (S4b). Only geometries S3 and S4a showed the requested behaviour in terms of input reflection coefficient within the entire 60–90 MHz frequency range. All other options were immediately discarded.

Figure 4 shows the most relevant geometrical solutions tested for the TE. Since the initial requirement about the frequency flexibility can be reached by radially shifting the TE itself, it was immediately evident that a folded (as for

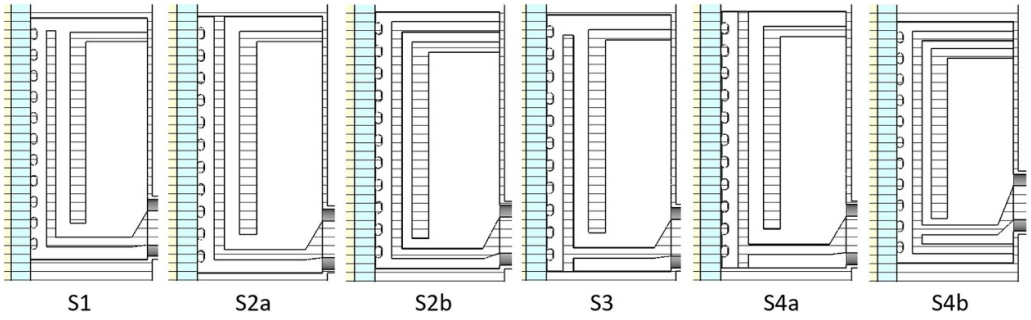

Figure 3. Tested solutions in terms of antenna strap shape.

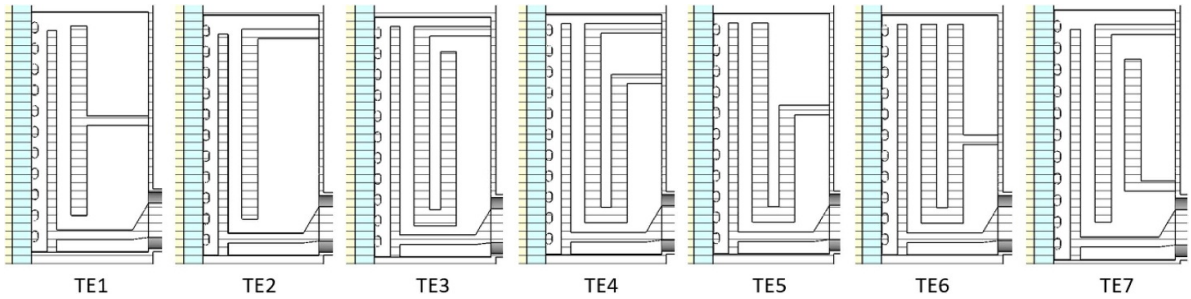

Figure 4. Tested solutions in terms of tuning elements.

instance TE3) or a double TE (as TE7) considerably reduced the radial dynamic, hence they had to be dropped. However, it is important to stress that for reduced frequency bandwidth applications (or even better for fixed frequency resonance), those TE designs could be successfully implemented.

Once the pool of strap (S3 or S4a) and TE (TE1 or TE2) candidates was considerably reduced by imposing the frequency flexibility, the analysis moved to the evaluation of the total electric field within the antenna box, which allowed to select the combined geometry S3TE2 as the most promising antenna to be optimized (see [11] for further details). Starting from a raw model, all strap and TE surfaces were smoothed and optimized to reduce the local electric fields. Figure 5 documents the electric field within the antenna box for both the starting raw geometry (top) and the optimized one (bottom). For both launchers, the electric fields were evaluated at the lower available resonance. To be more specific, the raw model was tested at 59.92 MHz, where a -12.5 dB S_{11} magnitude allowed to couple 755 kW out of the 800 kW assumed as incident power. The optimized model was tested at 61.44 MHz instead, where a -7.7 dB S_{11} magnitude allowed to couple 664 kW out of the same incident power. The optimization process allowed for considerably reducing the electric field in the most critical areas, above all around the TE surfaces.

It must be stressed that while the electric field average behaviour is correctly predicted once the simulation has reached convergence, the electric field maxima are influenced by how curved items are built and then discretized instead; different construction choices (for instance analytical curve defined by the user vs. built-in round-up procedure automatically performed by the tool) may lead to slightly different maxima. As a consequence, a more reliable indication of the exact field maxima should come from measurements of a mock-up antenna in a suitable environment. Our strategy would be to work below the safety limit and test the mock-up in the most realistic conditions to check that, after usual preparation works (surface cleaning, low-power test of resonances with a seawater load, baking, voltage test in vacuum tank, conditioning), no arcing occurs. If this is not the case, a post-test identification of arcing location(s) has(ve) to be carried out and compared with simulation model and predictions. Due to above mentioned uncertainties, the analysis of the parallel electric fields in front of the launcher has not been addressed yet. The authors are fully aware that this is a critical parameter in trying to minimize impurity production; however, any further geometrical optimization (above all of the front face) should be done only after a consistency check of the exact field maxima.

3.3. Frequency analysis

Keeping constant the geometry, the TE was radially shifted backwards to verify the frequency coverage; figure 6 reports the position of the resonance according to the radial displacement of the TE (in cm). The reader can notice that a first resonance driven by the radial position of the TE covers the range 60–85 MHz; a second resonance appears around 90 MHz and it is only slightly influenced by the TE radial position. Table 1 shows the magnitude of the maximum electric field (in MV m^{-1}) evaluated for different antenna sections (same

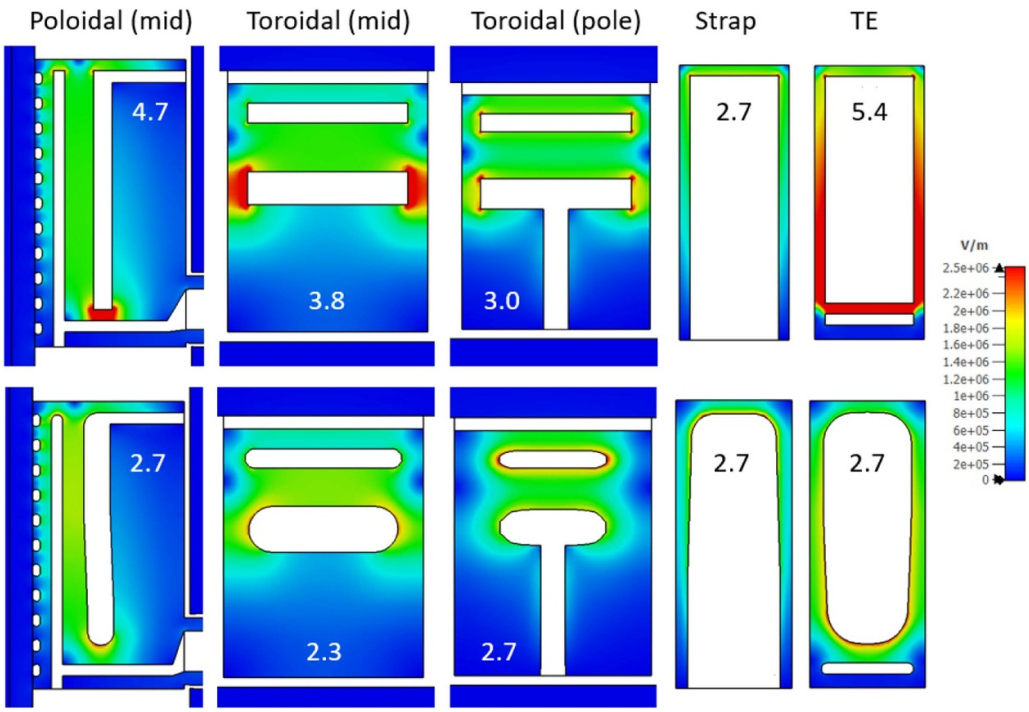

Figure 5. Magnitude of the max electric field (clamped to 2.5 MV m^{-1}) evaluated with CST-MWS for different antenna sections, given 800 kW of incident power at the lower available resonance. From left to right, the fields are plotted at the poloidal mid-section, at the toroidal mid-section, at the toroidal position of the TE pole, at the radial mid-section of the strap, at the radial mid-section of the TE. The top row reports the electric field computed for the starting model, and the bottom one the electric field computed for the optimized launcher. The maximum electric field for each section (as indicated by CST-MWS) is also reported on the picture, expressed in MV m^{-1}.

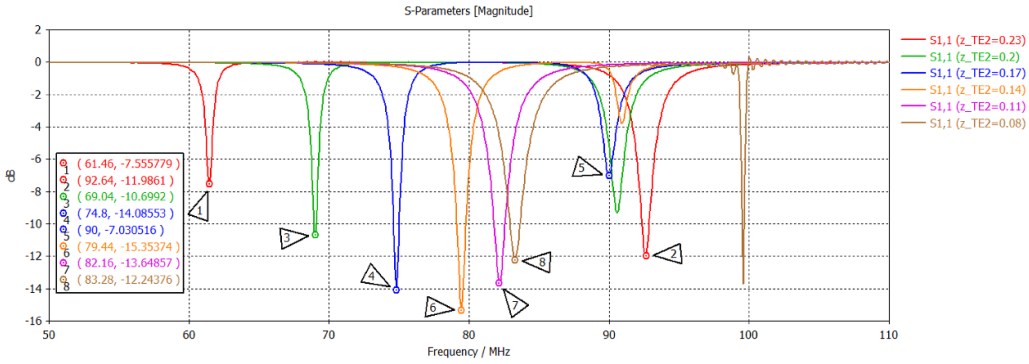

Figure 6. Magnitude of the input reflection coefficient for different TE radial positions (expressed in cm). The curve corresponding to z_TE2 = 0.08 cm shows a ripple around the 100 MHz minimum; despite no warning from the software, this behaviour probably indicates that, at the frequency, the mesh is not accurate enough. This point has been added only to show that a second minimum appears for every TE position, but it is not of interest here being above the 90 MHz upper limit of operation.

Table 1. From left to right: resonance frequency (MHz), magnitude of the input reflection coefficient (in dB), coupled power (in kW) given 800 kW of incident power, magnitude of the maximum electric field at the poloidal mid section, at the toroidal mid section, at the toroidal position of the TE pole, at the radial mid section of the strap, at the radial mid section of the TE.

f_{res}	$\lvert S_{11}\rvert$	$P_{coupled}$	Pol. mid	Tor. mid	Tor. pole	Strap	TE
61.44	−7.7	664	2.7	2.3	2.7	2.7	2.7
67.92	−10.3	726	2.9	2.4	2.6	2.7	2.8
74.80	−14.1	796	3.1	2.1	3.0	3.1	2.6
75.20	−6.1	603	2.8	1.9	2.5	2.5	2.3
82.16	−13.6	765	3.2	2.2	3.0	2.9	1.0
90.56	−9.3	706	3.1	2.3	3.0	3.1	1.4

Table 2. From left to right: vacuum layer size (cm), resonance frequency (MHz), magnitude of the input reflection coefficient (in dB), coupled power (in kW) given 800 kW of incident power, magnitude of the maximum electric field at the poloidal mid section, at the toroidal mid section, at the toroidal position of the TE pole, at the radial mid section of the strap, at the radial mid section of the TE.

Vacuum	f_{res}	$\lvert S_{11}\rvert$	$P_{coupled}$	Pol. mid	Tor. mid	Tor. pole	Strap	TE
0.00	62.48	−1.3	202	0.7	0.6	0.6	0.6	0.7
6.08	61.44	−7.7	664	2.7	2.3	2.7	2.7	2.7
10.00	61.28	−19.1	790	4.1	3.4	4.2	4.3	4.1
10.00	61.12	−7.1	644	3.3	3.2	3.8	3.8	3.6
20.00	61.12	−11.1	739	6.0	4.9	5.8	5.9	5.7

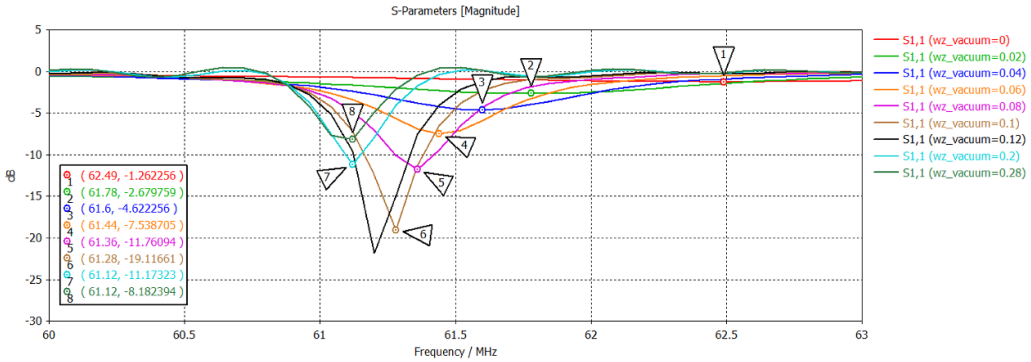

Figure 7. Magnitude of the input reflection coefficient for different radial extensions of the vacuum layer (in cm).

as in figure 5), given 800 kW of incident power, along the required frequency range; the resonance frequency (in MHz) is reported on the first column, while the magnitude of S_{11} (in dB) and the coupled power to the load (in kW) are listed in columns two and three respectively. In general, the electric field is slightly higher on the strap while moving to higher frequencies, while it decreases all around the TE. It should also be stressed that the geometrical optimization described in section 3.2 was performed at the lower available frequency, hence it is not so surprising that the minimum electric fields are found there. Apart from further geometrical optimization, one possible strategy to reduce the local electric fields is to operate slightly off the main resonance. For instance, instead of using the 74.80 MHz resonance, one could tune the working frequency to 75.20 MHz keeping constant the position of the TE, with all the benefits listed in table 1; this has unfortunately a negative impact in terms of reduction of the coupled power.

3.4. Load resilience

Similarly to section 3.3, we tested the antenna behaviour for different loading conditions, changing the amount of vacuum between the antenna mouth and the lossy dielectric layer. Figure 7 documents the effect of the vacuum layer radial extension on the input reflection coefficient; the resonance frequency is only mildly affected by the amount of vacuum (±0.5 MHz), while its intensity goes from about −1 dB to more than −20 dB. It must be stressed that a huge radial variation (up to 28 cm) has been taken into account with the only purpose to show that there is an optimal radial distance of the launcher in terms of input parameters. The minimal effect on resonance frequency implies that the tuning (i.e. TE position) needs not be adjusted if the loading suddenly changes within a shot; as a consequence, while the radial movement of the TE has to cover the whole frequency range, no action of this sort has to be necessarily performed in real-time. Conversely, the possibility to radially displace the entire antenna during a shot, and therefore to increase (or decrease) the antenna-plasma distance, appears very beneficial to optimized coupled power. Similarly, figure 9 indicates that, at least at this stage, a TMS should be in place to protect the feeding lines in case of a sudden drop in the input reflection coefficient. To conclude the analysis, table 2 reports the electric field maxima for some configurations; as previously stated, operating the antenna slightly off-resonance has a beneficial impact on local electric fields.

3.5. Analysis in front of a plasma with TOPICA code

The final step of this preliminary analysis was the simulation with TOPICA code [12] of the optimized launcher described in the previous sections. This study focused on the lower frequency resonance (as predicted by CST-MWS and shown in figure 6) and it aimed at completing figure 7 with a realistic

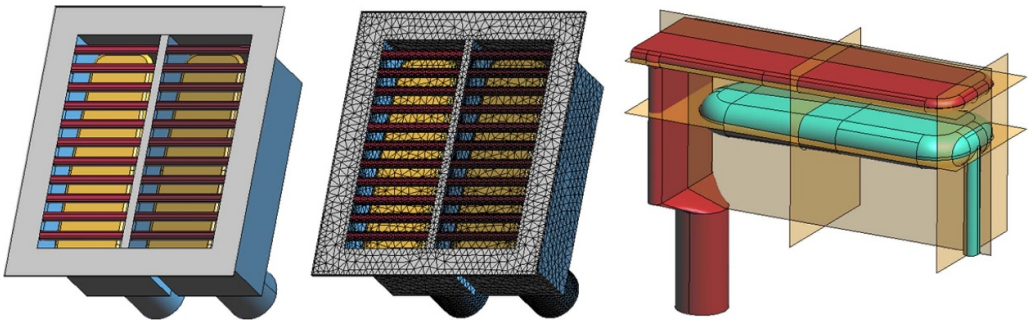

Figure 8. Front view of the IC launcher simulated with TOPICA (left) with a detail of the mesh resolution on the metallic surfaces (middle) and a zoomed view of the strap and tuning element (right). The position of the surfaces where the electric near field has been tested are reported on the right picture too.

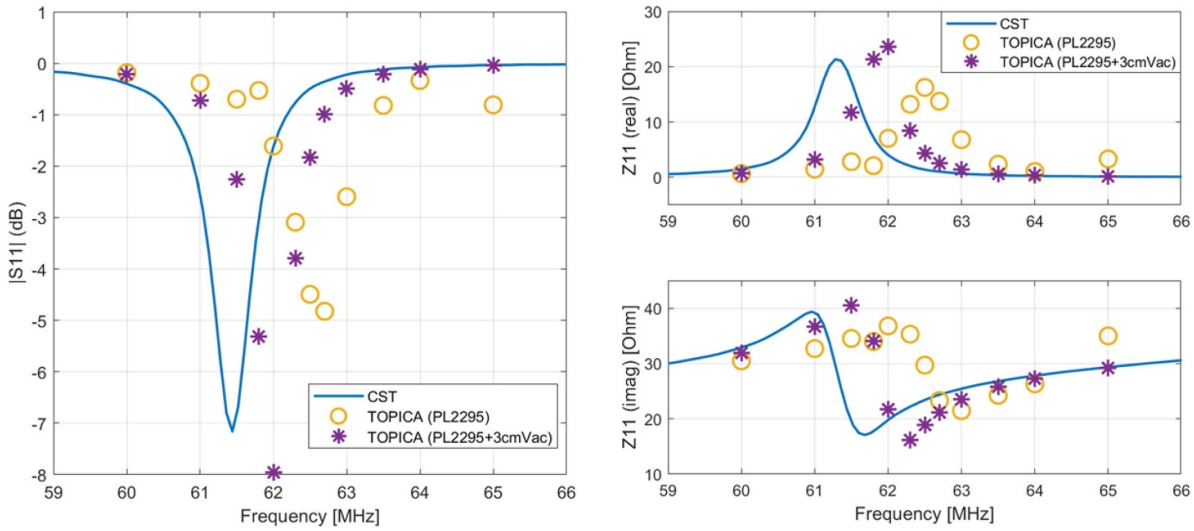

Figure 9. S11 magnitude (left) and input impedance (real part top-right, imaginary part bottom-right) as a function of frequency for the optimized launcher with the reference plasma profile and the shifted one loaded in TOPICA. The CST-MWS curve corresponding to the lower frequency resonance in figure 6 is added for comparison.

plasma profile. As anticipated, the full 2-strap antenna has been included in TOPICA model. Figure 8 reports a front view of the selected launcher and a detailed one of the adopted strap and TE.

The kinetic profiles of the single null, 6 T, 5.5 MA, reference scenario with Neon seeding, predicted by integrated modelling simulations [13], were joint with those predicted by edge simulations in plasma detachment condition [14] and given as input to TOPICA (see also [4] for additional details). Figure 9 shows the comparison between CST-MWS predictions with equivalent dielectric load and TOPICA simulations with this realistic plasma profile (labelled as shot 2295 in the picture). To provide a better insight into the load dependence, the plasma profile has also been shifted away from the antenna by adding 3 cm of vacuum. As already highlighted by figure 7, different loading conditions can imply a small shift in the resonance frequency (less than one MHz). Moreover, figure 9 proves that a first geometrical optimization of the launcher can be pursued also with an equivalent dielectric, while a verification with actual plasma operation remains clearly mandatory.

To conclude the analysis with TOPICA, figure 10 compares the near fields within the antenna box in CST-MWS (top) and in TOPICA (middle and bottom), always evaluated at the corresponding lower frequency resonance. More specifically, in CST-MWS the resonance occurs at 61.44 MHz with a -7.2 dB S_{11} magnitude, allowing to couple about 646 kW per port out of the 800 kW assumed as incident power per port. For the reference plasma profile in TOPICA (bottom), the resonance occurs at 62.8 MHz with a -4.8 dB S_{11} magnitude (about 469 kW coupled per port), while for the 3 cm shifted profile (middle) the resonance moves to 62.0 MHz with a -7.96 dB S_{11} magnitude (679 kW coupled per port). In terms of maximum field within the antenna box, CST-MWS reports a peak of 2.7 MV m^{-1}, while 2.5 MV m^{-1} and 2.0 MV m^{-1} are found for the shifted plasma and the reference plasma in TOPICA, respectively.

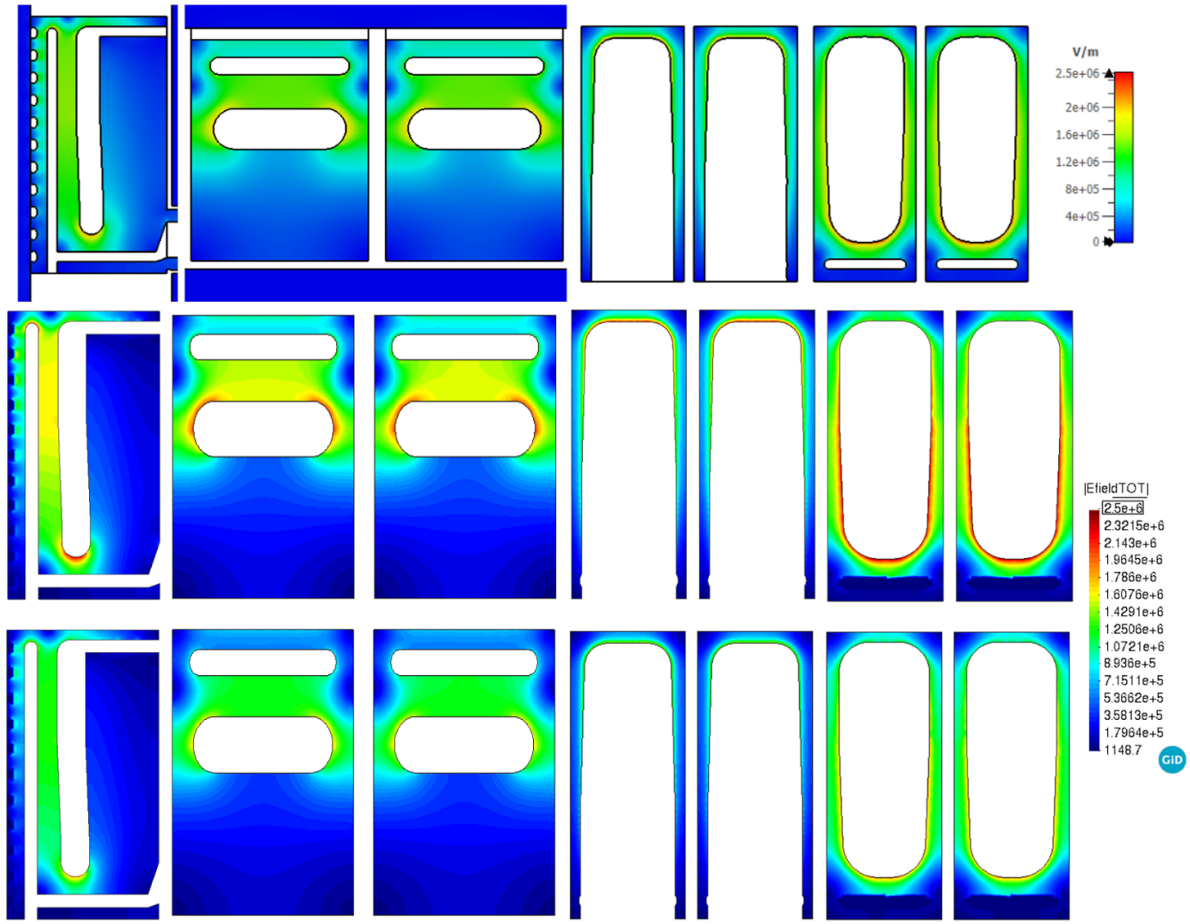

Figure 10. Magnitude of the max electric field (clamped to 2.5 MV m^{-1}) evaluated with CST-MWS (top), TOPICA (reference plasma with 3 cm additional vacuum, middle) and TOPICA (reference plasma, bottom) for different antenna sections, given 800 kW of incident power per port at the lower available resonance. From left to right, the fields are plotted at the poloidal mid-section, at the toroidal mid-section, at the radial mid-section of the strap, at the radial mid-section of the TE.

4. Conclusions and perspectives

This paper presented a full-metal tunable self-resonant antenna concept and its application to the case study of the DTT experiment. Several topologies were first tested and a promising candidate was selected. The proposed launcher can be tuned to resonate from 60 MHz to 90 MHz, guaranteeing a low input reflection coefficient throughout the entire frequency bandwidth; it also shows an encouraging resilience in the case of real plasma operations. A first estimate of the local electric fields within the antenna box indicated that further geometrical optimization is required to successfully operate the antenna with a sufficient confidence margin within the 2.5 MV m^{-1} limit adopted during the design phase.

ORCID iDs

D. Milanesio https://orcid.org/0000-0002-5114-7235
D.L. Galindo Huertas https://orcid.org/0000-0002-4289-9996
B. Baiocchi https://orcid.org/0000-0002-1483-3113
A. Cardinali https://orcid.org/0000-0003-4606-9903
D. Mascali https://orcid.org/0000-0003-3861-1547
A. Pidatella https://orcid.org/0000-0002-3661-8537

References

[1] Lin Y., Wright J.C. and Wukitch S.J. 2020 *J. Plasma Phys.* **86** 865860506
[2] Tran M. *et al* 2022 *Fusion Eng. Des.* **180** 113159
[3] Ambrosino R. 2021 *Fusion Eng. Des.* **167** 112330
[4] Ceccuzzi S. *et al* 2023 *AIP Conf. Proc.* **2984** 030015
[5] Mirizzi F. *et al* 2023 *Fusion Eng. Des.* **191** 113788
[6] Balanis C. 2005 *Antenna Theory: Analysis and Design* (Wiley)
[7] Hansen R.C. and Collin R.E. 2011 *Electrically Small Antennas: Canonical Types* (Wiley) (https://doi.org/10.1002/9781118106860)
[8] Milanesio D., Maggiora R. and Dassano G. 2020 *AIP Conf. Proc.* **2254** 070011
[9] Cardinali A., Baiocchi B., Castaldo C., Bilato R., Brambilla M., Casiraghi I., Ceccuzzi S., Napoli F.,

Ravera G.L. and Tuccillo A.A. 2022 *J. Phys.: Conf. Ser.* **2397** 012017
[10] Martone R., Albanese R., Crisanti F., Martin P. and Pizzuto A. 2019 Divertor tokamak test facility: interim design report *Technical Report* (DTT) (available at: www.dtt-dms.enea.it/share/s/avvglhVQT2aSkSgV9vuEtw)
[11] Milanesio D. *et al* 2023 *AIP Conf. Proc.* **2984** 060009
[12] Milanesio D., Meneghini O., Lancellotti V., Maggiora R. and Vecchi G. 2009 *Nucl. Fusion* **49** 115019
[13] Casiraghi I. *et al* 2021 *Nucl. Fusion* **61** 116068
[14] Innocente P., Ambrosino R., Brezinsek S., Calabrò G., Castaldo A., Crisanti F., Dose G., Neu R. and Roccella S. 2022 *Nucl. Mater. Energy* **33** 101276